Chemical Senses, 2019, Vol 44, 497–505
doi:10.1093/chemse/bjz044
Original Article
Advance Access publication 5 July 2019

OXFORD

Original Article

The Effect of Calcium Buffering and Calcium Sensor Type on the Sensitivity of an Array-Based Bitter Receptor Screening Assay

Margriet Roelse[1,2,3,*], Ron Wehrens[1,4], Maurice G.L. Henquet[1], Renger F. Witkamp[3], Robert D. Hall[1,2] and Maarten A. Jongsma[1]

[1]BU Bioscience, Wageningen University and Research, Droevendaalsesteeg 1, 6708 PB Wageningen, The Netherlands, [2]Laboratory of Plant Physiology, Wageningen University and Research, Droevendaalsesteeg 1, 6708 PB Wageningen [3]Nutritional Biology and Health, Wageningen University and Research, Stippeneng 4, 6708 WE Wageningen, The Netherlandsand [4]BU Biometris, Wageningen University and Research, Droevendaalsesteeg 1, 6708 PB Wageningen

*Correspondence to be sent to: Margriet Roelse, BU Bioscience, Wageningen University and Research, Droevendaalsesteeg 1, 6708 PB Wageningen, The Netherlands. e-mail: margriet.roelse@wur.nl

Editorial Decision 1 July 2019.

Abstract

The genetically encoded calcium sensor protein Cameleon YC3.6 has previously been applied for functional G protein–coupled receptor screening using receptor cell arrays. However, different types of sensors are available, with a wide range in [Ca^{2+}] sensitivity, Hill coefficients, calcium binding domains, and fluorophores, which could potentially improve the performance of the assay. Here, we compared the responses of 3 structurally different calcium sensor proteins (Cameleon YC3.6, Nano140, and Twitch2B) simultaneously, on a single chip, at different cytosolic expression levels and in combination with 2 different bitter receptors, TAS2R8 and TAS2R14. Sensor concentrations were modified by varying the amount of calcium sensor DNA that was printed on the DNA arrays prior to reverse transfection. We found that ~2-fold lower concentrations of calcium sensor protein, by transfecting 4 times less sensor-coding DNA, resulted in more sensitive bitter responses. The best results were obtained with Twitch2B, where, relative to YC3.6 at the default DNA concentration, a 4-fold lower DNA concentration increased sensitivity 60-fold and signal strength 5- to 10-fold. Next, we compared the performance of YC3.6 and Twitch2B against an array with 11 different bitter taste receptors. We observed a 2- to 8-fold increase in sensitivity using Twitch2B compared with YC3.6. The bitter receptor arrays contained 300 spots and could be exposed to a series of 18 injections within 1 h resulting in 5400 measurements. These optimized sensor conditions provide a basis for enhancing receptomics calcium assays for receptors with poor Ca^{2+} signaling and will benefit future high-throughput receptomics experiments.

Key words: calcium, cell array, GPCR, HTS screening, TAS2R

Introduction

Bitter taste receptors (T2Rs or TAS2Rs) are a class of G protein–coupled receptors (GPCRs), for which 25 subtypes have now been identified in the human genome. Some are broadly tuned (e.g., TAS2R10, -14, -46), whereas others are more specific (e.g., TAS2R3, -5, -9, -13, -20, -41, -45, -50). Next to this, there are also 4 still remaining with an orphan status (TAS2R19, -42, -45, -60) (Behrens 2013, #194). Interestingly, their expression and downstream

signaling is not limited to the oral cavity and has been found to include other parts of the gastrointestinal tract, respiratory and genitourinary systems, and brain and immune cells (Devillier et al. 2015; Lu et al. 2017). These findings suggest roles beyond taste, which is further fueling the search for endogenous and exogenous ligands.

In screening assays used thus far, a number of bitter receptors have shown poor signals that could be related to variable functional expression on the cell membrane (Bufe et al. 2004) (Chandrashekar et al. 2000; Behrens et al. 2006; Reichling et al. 2008; Kuhn et al. 2010). Receptors with lower functional expression may suffer from poor transport to or rapid internalization from the cell membrane (Behrens et al. 2006), may have poor glycosylation (Reichling et al. 2008) and with certain levels of constitutive activity may become phosphorylated by receptor kinases that target them for β-arrestin internalization and may become generally exhausted for signaling (Ozeck et al. 2004). Also, when comparing cytosolic calcium signaling of neuropeptide receptor 1 (NK1) to the relatively strongly responding bitter receptor 8 (TAS2R8), we found that the signal amplitude for TAS2R8 was approximately 3-fold lower than for the NK1 receptor (Roelse et al. 2018). When signals are low, it is important to use a probe that is the most sensitive in the resting range of cytosolic calcium levels. Previously, in reverse transfected arrays with bitter receptors, calcium assays were performed using the Cameleon YC3.6 sensor protein because of its wide dynamic range (5- to 6-fold change in the ratio of YFP/CFP upon Ca^{2+} binding in vitro) and brightness (Nagai et al. 2004; Miyawaki et al. 2013). The arrays were typically printed using 2 plasmids at identical concentrations: one encoding the GPCR and one the calcium-sensing protein. However, the effect of the concentration and type of sensor protein on the sensitivity and signal strength of the assay were not previously considered.

Since the first use of Cameleon calcium sensors (Miyawaki et al. 1997), many variants of this ratiometric calcium probe have been described that are also based on the response of the FRET pair CFP and YFP (Mank and Griesbeck 2008; Zhao et al. 2011). The palette of probes involves various modifications: the CFP and YFP proteins have been optimized to enhance their spectral properties (Goedhart et al. 2012), the YFP protein has been circularly permutated (Nagai et al. 2004), the linker between CFP and YFP has been varied in length (Horikawa et al. 2010), and the calcium binding modality has been changed from calmodulin to troponin (Thestrup et al. 2014). Ratio imaging of YFP and CFP is advantageous because it is, in principle, independent of the expression level of the calcium sensor, and thus a direct reporter of the actual calcium concentration. For a receptomics platform, this is relevant because the genetically encoded calcium sensor is transiently expressed in a receptor cell array which results in highly variable expression levels between cells within a spot. The genetically encoded property of this fluorescent probe further allows the identification of transfected cells prior to the start of the experiment and the correct positioning of the array under the microscope. Fluorescent calcium sensor proteins such as the GECO probes (Zhao et al. 2011) only show significant fluorescence emission upon calcium increase. This yields very low fluorescent signals of the array prior to the start of a GPCR activation experiment, which is more difficult to focus, position, and analyze.

In this study, we aimed to evaluate ratiometric probes with a calcium affinity that would ensure sufficient sensitivity for relatively minor calcium transients of bitter taste receptors above the resting levels of ~100 nM in HEK293 cells (Tong et al. 1999). *Cameleon YC3.6 (Nagai et al. 2004; Horikawa et al. 2010; Miyawaki et al. 2013), Nano140 (Horikawa et al. 2010), and Twitch2B (Thestrup et al. 2014) have K_d values of ~140–250 nM that fit this criterion in principle, but these probes are distinctly different: YC3.6 and Nano140 both include a modified calmodulin domain, but with different cooperative binding and dissociation constants, and Twitch2B contains a troponin domain with only one calcium binding pocket and a more linear calcium binding curve. An added advantage of the use of troponin over calmodulin is that it does not potentially interact with host cell calmodulin binding proteins (Mank and Griesbeck 2008). Next to sensor type, we also aimed to evaluate the effect of the cytosolic sensor concentration because a high sensor concentration may increase signal-to-noise levels, but may also result in a lower signal intensity because of calcium buffering (Miyawaki et al. 2013; Rose et al. 2014).

Materials and methods

Expression vectors

Reverse transfected cell arrays were prepared and analyzed as previously described in Roelse et al. (2018). The genes encoding TAS2R1, TAS2R3, TAS2R4 (both FVS and SLN variants), TAS2R8, TAS2R10, TAS2R14, TAS2R16, TAS2R38 (both PAV and AVI variants), TAS2R39, TAS2R43, and TAS2R46 (see Supplementary Table 1 for sequence information) were obtained from genomic DNA of HEK293 cells by PCR amplification and were cloned into pcDNA3 containing the N-terminal sstr3 tag (gift from Dr. Wolfgang Meyerhof, German Institute of Human Nutrition Potsdam-Rehbrücke, Germany). Plasmid, pcDNA YC3.6 was obtained from Prof. Roger Tsien (UC San Diego). Yellow Cameleon-Nano140 pcDNA3 was a gift from Takeharu Nagai (Addgene plasmid # 51966), Twitch2B pcDNA3 was a gift from Oliver Griesbeck (Addgene plasmid # 49531).

Receptomics assay

DNA arrays comprising 15 × 19 spots were printed and processed as previously described (Roelse et al. 2018). Reverse transfected cell arrays were prepared using HEK293 cells stably transfected with Gα16GUST44 (a gift from Dr. Takashi Ueda, Nagoya City University, Nagoya, Japan). At 48 h after transfection, the cell arrays were taken from the incubator, washed, and incubated in assay buffer for 1 h prior to the measurements. Spots then were typically composed of 25–50 cells and imaged by a similar number of pixels. All measurement series were performed using a ~150 µL flowcell in the flowcell holder (Micronit Microfluidics B.V., Fluidic Connect PRO Chip Holder). The assay buffer C1 (NaCl 130 mM, KCl 5 mM, Glucose 10 mM, $CaCl_2$ 2 mM, HEPES 10 mM at pH 7.4) was set at a continuous flow of 300 µL/min across the array and sample injections were performed with a volume of 150 µL (Waters 2795 autosampler). Agonists used in the injections were ATP (Sigma A6419), chloramphenicol (Duchefa C0113.0100), aristolochic acid (Sigma A5512), denatonium benzoate (Wako 046-23561), picrotoxinin (Sigma P8390), PROP (Sigma P3755), and D-salicin (Wako 199-00083). The arrays were imaged by a Leica fluorescent stereo microscope (Leica M205FA with DFC 345 FX camera and 2.0× PlanApo objective with NA 0.35) fitted with a 0.32× C-Mount and filters for CFP (ET CFP 10447409, excitation 436/20, and emission 480/40) and YFP FRET (ET FRET 10450566, excitation 436/20, and emission 535/30). Lamp intensity (Osram, HXP-R 120W/45C VIS) was set at maximum, and the exposure time was 400 ms.

R_{min} and R_{max} measurement

The R_{min} and R_{max} signals were measured in a reverse transfected cell array containing mock transfected spots with either Twitch2B or YC3.6, according to the method described in McCombs and Palmer

(2008). In short, the array was equilibrated applying a 200 µL/min flow of C1 buffer for 10 min. First a blank injection of 300 µL C1 buffer was performed followed by a 300-µL injection with R_{min} buffer (C1 buffer without $CaCl_2$ but supplemented with 3mM ethyleneglycol-bis(aminoethylether)-tetraacetic acid [EGTA] and 5 µM ionomycin [Sigma I0634] adjusted to pH 7.4 using NaOH). One minute after the R_{min} injection, when the R_{min} buffer exposure was maximal, the flow was stopped for 15 min to allow the cells to become fully calcium ion depleted. Next, the flow was restarted replacing the R_{min} buffer with the C1 buffer and cells were equilibrated again in the C1 buffer for 10 min. Subsequently, 300 µL of R_{max} buffer (C1 buffer with instead 5 mM $CaCl_2$ and 5 µM Ionomycin) was injected into the flow and the flow was again stopped after 1 min. Cells were then again left for 10 min to become fully calcium saturated allowing the measurement of R_{max}.

Calcium affinity curves were calculated using a Hill coefficient calculation modified from Gadagkar and Call (2015):

$$F(S) = R_{\min} + (\Delta_{\max} \times S^n)/(K_d^n \times S^n)$$

R_{min} = minimal YFP/CFP ratio, Δ_{max} = difference between R_{min} and R_{max}, S = calcium concentration [Ca^{2+}], n = Hill coefficient, K_d = EC_{50} calcium value of the sensors.

Hill coefficient and K_d values were used from literature sources. Twitch2B has a K_d of 200 nM and Hill coefficient of 1.3 according to (Thestrup et al. 2014). For YC3.6, conflicting values have been published. The initial publication states a K_d of 250 nM and a Hill coefficient of 1.7 (Nagai et al. 2004). However, a more thorough study performed by Horikawa et al. (2010) showed a bi-phasic calcium affinity curve for YC3.6 with a high-affinity range of K_d of 215 nM and Hill coefficient of 3.6, and a low-affinity range of K_d of 780 nM and Hill coefficient of 1.2. Here, we used the high-affinity range of K_d of 215 nM and Hill coefficient of 3.6 to plot a comparative curve.

Data analysis

The analysis of data from the receptor cell arrays was performed as described in Wehrens et al. (2019). In short, FRET images for the CFP and YFP channels were recorded and converted, using the CellProfiler software package (Kamentsky et al. 2011), into raw CFP and YFP intensity values. Spots with less than 15 fluorescent pixels and spot types with fewer than 5 replicates were removed from the data analysis. After smoothing and interpolation to remove the differences in timing between the CFP and YFP measurements, spot signals were calculated as the ratio of the CFP and YFP values. These signal peak heights associated with individual injections were calculated as the difference between start and maximal ratio value in the spot signal within a time window of 30 cycles (just under 2 min). A representative example is shown in the supplementary data to Wehrens et al. (2019). These signal peak heights, after log-scaling were then used in a mixed model with the injection type as fixed variable, and spot number as random variable. This greatly improves statistical power because the between-spot variation is eliminated. Results presented in the figures consist of treatment-versus-control contrasts, with the blank injection as the control, after back-transformation to the original scales. This leads to coefficients that should be interpreted as multiplicative effects: a value of 1.1 should be interpreted as a 10% increase in response compared with the reference. A value of 1.0 indicates no difference to the reference. Depending on the goal or characteristics of the experiments, different choices for reference injections are possible: like blank injection(s) or a sample contrast as in Wehrens et al. (2019).

Results

Effect of sensor type and relative sensor concentration

On a receptor cell array, 3 sensor types (YC3.6, Nano140, and Twitch2B) and 2 receptor types (TAS2R8 and TAS2R14) were combined in different configurations. The sensor plasmids were printed at 3 concentrations (8, 16, and 25 ng/µL), while keeping the receptor coding DNA (25 ng/µL) concentration constant. Empty vector DNA was added to maintain the same total DNA concentration (50 ng/µL). The receptor cell array was exposed to increasing concentrations of a mixture of chloramphenicol and picrotoxinin, selective ligands for TAS2R8 and TAS2R14, respectively. The experiment was repeated twice using different cell arrays. Figure 1 shows an example of the raw traces of an injection series for TAS2R8 and TAS2R14, representing all 3 sensor types at a concentration of 16 ng/µL.

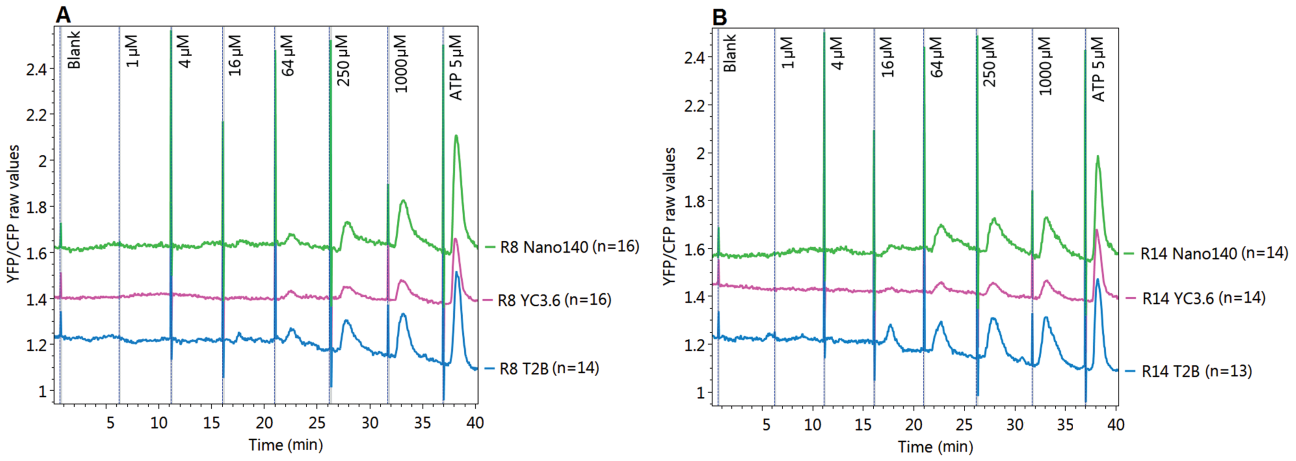

Figure 1. Averaged raw traces of TAS2R8 (**A**) and TAS2R14 (**B**) in an injection series of increasing chloramphenicol and picrotoxinin concentrations (array 2). Samples were injected sequentially at intervals of 5 min and with an exposure time of approximately 30 s. The ligand concentrations were as indicated in the chart. The lines represent averages of 13–16 replicated spots as indicated in the legends of the charts. In this example, the 3 sensors were printed at a concentration of 16 ng/µL DNA.

After the blank injection, response peaks increased with increasing ligand concentrations for all 3 sensor types and for both bitter taste receptors. The final injection was a positive control injection with ATP at 5 µM. The purinergic receptors, endogenously expressed in the HEK293 host cell, are activated by ATP showing a clear positive control peak for all spot types. An additional 12 curves were obtained in parallel for the other sensor concentrations. The results are summarized in 18 replicated dose–response curves derived from the 2 arrays in 2 × 40 min (Figure 2). These response curves, including 95% confidence intervals, are shown in Supplementary Figure 1.

The curve values represent estimates of treatment-versus-control contrasts with respect to the 1 µM agonist injection, the lowest sample dilution which does not evoke a specific response signal. In this case, the injection with the lowest concentration was chosen as the reference because the blank injection in one of the arrays gave an artifact response, probably due to inadequate pre-washing of the auto sampler. Spot-based contrasts were determined to reduce the variation between the spots. The red and blue curves represent replicated experiments using 2 different arrays. The results for the 2 arrays are in good agreement, taking into account the width of the confidence intervals shown in Supplementary Figure 1. In both experiments with TAS2R8, the Twitch2B sensor at a gene dose of 8 ng/µL gave the highest signal and sensitivity. For TAS2R14, with responses double those of TAS2R8, the effects were less pronounced but nevertheless still visible.

The effects of sensor type and sensor concentration are summarized in Table 1. Responses are based on treatment-versus-control contrasts compared with a nonresponse or blank treatment (1 µM agonist in this case): a value of 1.1 should be interpreted as a 10% increase in response compared with the reference, and a value of 1.0 indicates no difference. Looking at a combined effect of sensor type and concentration, YC3.6 at 25 ng/µL (standard in Roelse et al. 2018) compared with Twitch2B at 8 ng/µL, when exposed to a 250 µM ligand concentration, results in an 11-fold signal increase from 0.018 to 0.203 for TAS2R8 and a 4- to 5-fold increase for TAS2R14 (0.021–0.093). The sensitivity increase is up to 60-fold with lowest significant detection at 16 µM instead of 1000 µM. Splitting the sensor and concentration effects, it is clear that all probes benefit 4- to 15-fold from the reduced probe concentration and that Twitch2B is generally up to 4-fold more sensitive than the other 2 probes.

Comparing YC3.6 and Twitch2B sensors

The striking improvement in response amplitude and sensitivity for the bitter receptors TAS2R8 and TAS2R14 using Twitch2B instead of YC3.6 led us to investigate whether this also held up for other members of the bitter taste receptor family. To evaluate this, an array with 11 different bitter taste receptor genes combined with both sensors at a gene dose of 8 ng/µL was prepared. The array consisted of the bitter receptors TAS2R1, TAS2R3, TAS2R4 (both FVS and SLN genotypes), TAS2R8, TAS2R10, TAS2R14, TAS2R16, TAS2R38 (both PAV and AVI genotypes), TAS2R39, TAS2R43, and TAS2R46 M228L. Two controls were present on the arrays: mock transfected spots to observe and correct for any TAS2R-independent host cell responses and YC- control spots. The YC- is a deletion

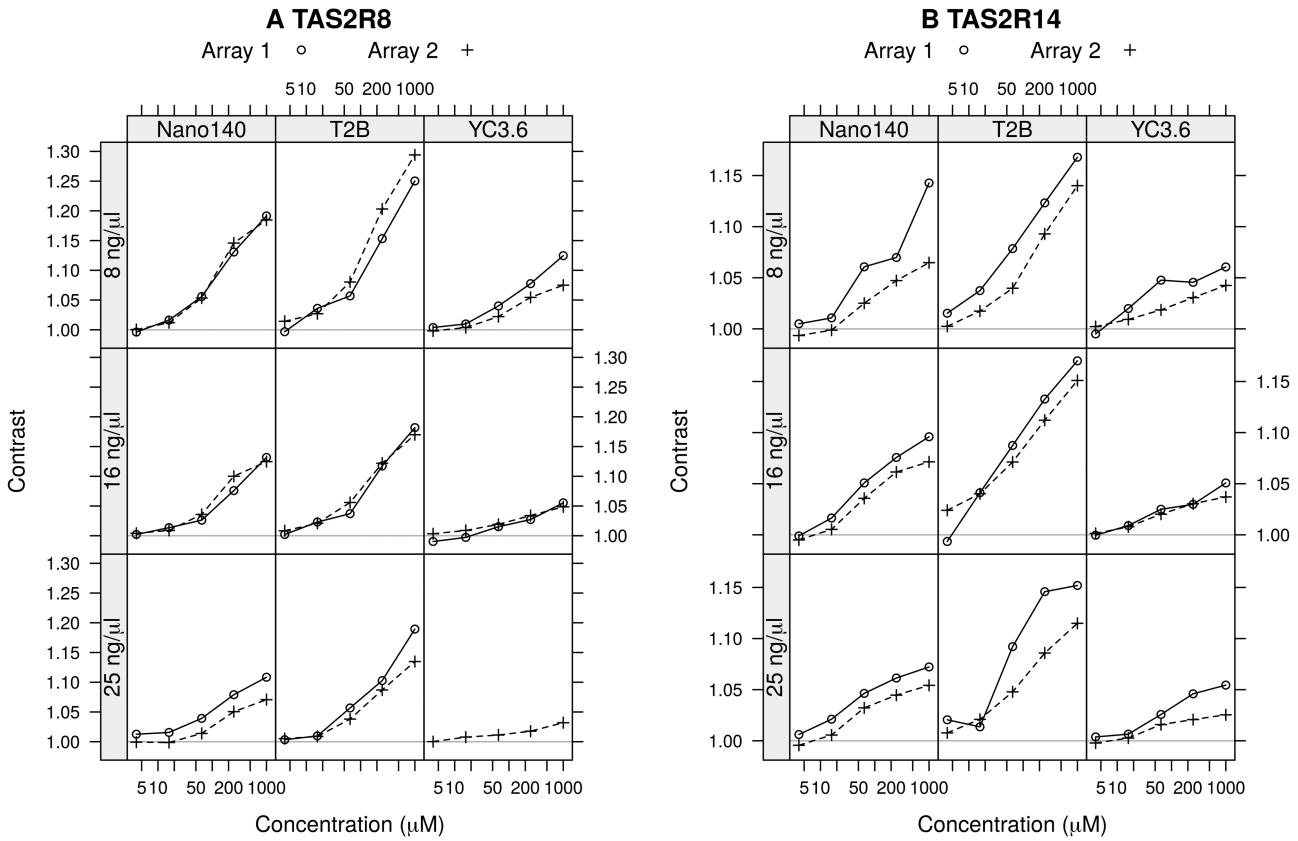

Figure 2. Response curves of TAS2R8 (**A**) and TAS2R14 (**B**) for stimulation with agonist mixture (chloramphenicol and picrotoxinin). (A) and (B) show agonist dose responses for the 3 sensor types at sensor gene dose of 8, 16, and 25 ng/µL. The 2 series represent 2 independent experiments. Response values represent estimates of treatment-versus-control contrasts with respect to the 1 µM injection. T2B, Twitch2B.

Table 1. Effects of sensor type and concentration

	TAS2R8		TAS2R14	
	Lowest detection[a]	Response at 250 µM[b]	Lowest detection	Response at 250 µM[b]
YC3.6 8 ng/µL	64 µM	1.054	250/64 µM	1.031
YC3.6 16 ng/µL	250/1000 µM	1.034	250/1000 µM	1.030
YC3.6 25 ng/µL	**1000 µM**	**1.018**	**1000/250 µM**	**1.021**
Nano140 8 ng/µL	64 µM	1.146	250/64 µM	1.047
Nano140 16ng/µL	64/250 µM	1.100	64 µM	1.061
Nano140 25ng/µL	250/64 µM	1.051	64 µM	1.045
Twitch2B 8 ng/µL	**16/64 µM**	**1.203**	64 µM	1.093
Twitch2B 16 ng/µL	64 µM	1.122	**16 µM**	**1.112**
Twitch2B 25 ng/µL	64 µM	1.087	64 µM	1.086

The most optimal and least optimal conditions are marked in bold.

[a]Detection threshold of agonist that gives a significant response in arrays 1 and 2 (see Supplementary Figure 1). When thresholds are different, both values of arrays 1 and 2 are given.

[b]Response estimate of array 1 for exposure to 250 µM agonist.

mutant of YC3.6 (Δ A332-S392) with fixed FRET between CFP and YFP to observe and correct for any optical effects of the samples during the fluorescence measurement. The receptors or empty vector (mock) were printed at a gene dose of 67 ng/µL reaching a total DNA concentration of 75 ng/µL that appeared optimal in a comparison of gene dosages from 50 to 150 ng/µL total DNA (Supplementary Figure 2). Receptor coding plasmid and total DNA concentration of the print mix was increased as a potential alternative way to improve the levels of functional receptor proteins present on the cell membrane (Roelse et al. 2018). The array contained 10 spot replicates of each bitter taste receptor, combined with either Twitch2B or YC3.6 at 8 ng/µL.

For each array, 2 dose–response experiments were performed by alternating agonist injections of pure compounds with increasing concentrations as shown in Figure 3. In total, 3 arrays were used to prepare the dose–response curves for 6 different agonists as presented in Figure 4. The agonist pairs were designed so that each would trigger a different receptor type. This resulted in a highly efficient throughput since in only 3 h of measurement time we were able to generate 150 dose–response curves and 12 mock or negative control curves (Supplementary Figure 3). Since each array contained 2 separate experiments, treatment-versus-control contrasts could be calculated with respect to the same blank injection, making it possible to obtain all results in a single analysis. The mock control did not show a significant response signal to any of the agonist doses confirming that the receptor responses that were observed are bitter receptor specific. In Table 2, the results are summarized indicating a response range for each receptor–agonist combination with either Twitch2B or YC3.6 as calcium sensor. Both sensor proteins were evaluated at similarly low DNA concentrations, but there is a 2- to 8-fold increase in sensitivity of Twitch2B compared with YC3.6. Some response signal exhaustion may have occurred in the series and the response peak height of the higher compound concentrations may be an underestimation. In Wehrens et al. (2019), we have shown how dosing order affects the peak height. In general, a repeated sample injection protocol can be incorporated into the analysis model to estimate the global decline of signal.

To check for metabolic exhaustion, a standard injection of ATP 5 or 10 µM was included at the end of each series. Such host cell responses triggered by ATP or Somatostatin-14 are normally used to check the vitality of the cells as they trigger the same IP_3 pathway via PLC1-4 (Wettschureck and Offermanns 2005; Narukawa et al. 2011; Lossow et al. 2016). Any changes in ATP response may indicate negative effects of the exposure to the standard bitter compounds. Supplementary Figure 4 shows the ATP response contrasts to the blank for each spot type on each array. Spot types with less than 5 spots were removed from the analysis (see also Supplementary Figure 3). The spot type–specific ATP signals did not significantly differ between the arrays showing no signs of metabolic exhaustion in these experiments. It is however relevant to notice that generally each spot type displays a different ATP response level that is usually lower than the mock. This has been shown before in Wehrens et al. (2019) and suggests negative interactions between bitter receptors and calcium signaling presumably independent of specific triggers (Wehrens et al. 2019).

Calcium response curves of YC3.6 and Twitch2B

Twitch2B and YC3.6 have similar dissociation constants of 200 and 215–250 nM, respectively, but they differ strongly in their Hill coefficient (1.3 vs. 3.6). To visualize the effect of the differences in Hill coefficient in the predicted calcium response curves of YC3.6 and Twitch2B, we measured the R_{min} and R_{max} of Twitch2B and YC3.6 using the method described in McCombs and Palmer (2008) (Figure 5A) and used a Hill coefficient calculation (Gadagkar and Call 2015) to estimate the response curves in relation to the calcium ion concentration (Figure 5B). The R_{min} buffer containing EGTA and ionomycin chelates all calcium ions resulting in a R_{min} ratio of 1.4 for YC3.6 and 0.8 for Twitch2B after about 15 min of exposure. Initially, after adding the R_{min} buffer, there was a spike in the ratio signal, showing the calcium depletion from the intracellular calcium stores. When the flow was started again and the R_{min} buffer was replaced by C1 buffer containing 2 mM $CaCl_2$, there was a large increase in the ratio signal of both sensors because of calcium reentering the cells. Twitch2B reached a R_{max} ratio of 2.6 and YC3.6 a R_{max} of 3.2 when exposed to the R_{max} buffer containing 5 mM $CaCl_2$ and 5 µM ionomycin. The dynamic range between R_{min} and R_{max} is quite comparable for both sensors, however, only Twitch2B clearly has a R_{min} well below the cells' resting level (around 100 nM; Tong et al. 1999). Only Twitch2B can therefore be used to record very small changes in calcium ion concentration both above and below the resting level. In addition, the Hill curves based on the respective Hill coefficients for Twitch2B and YC3.6 (Figure 5B) confirm this.

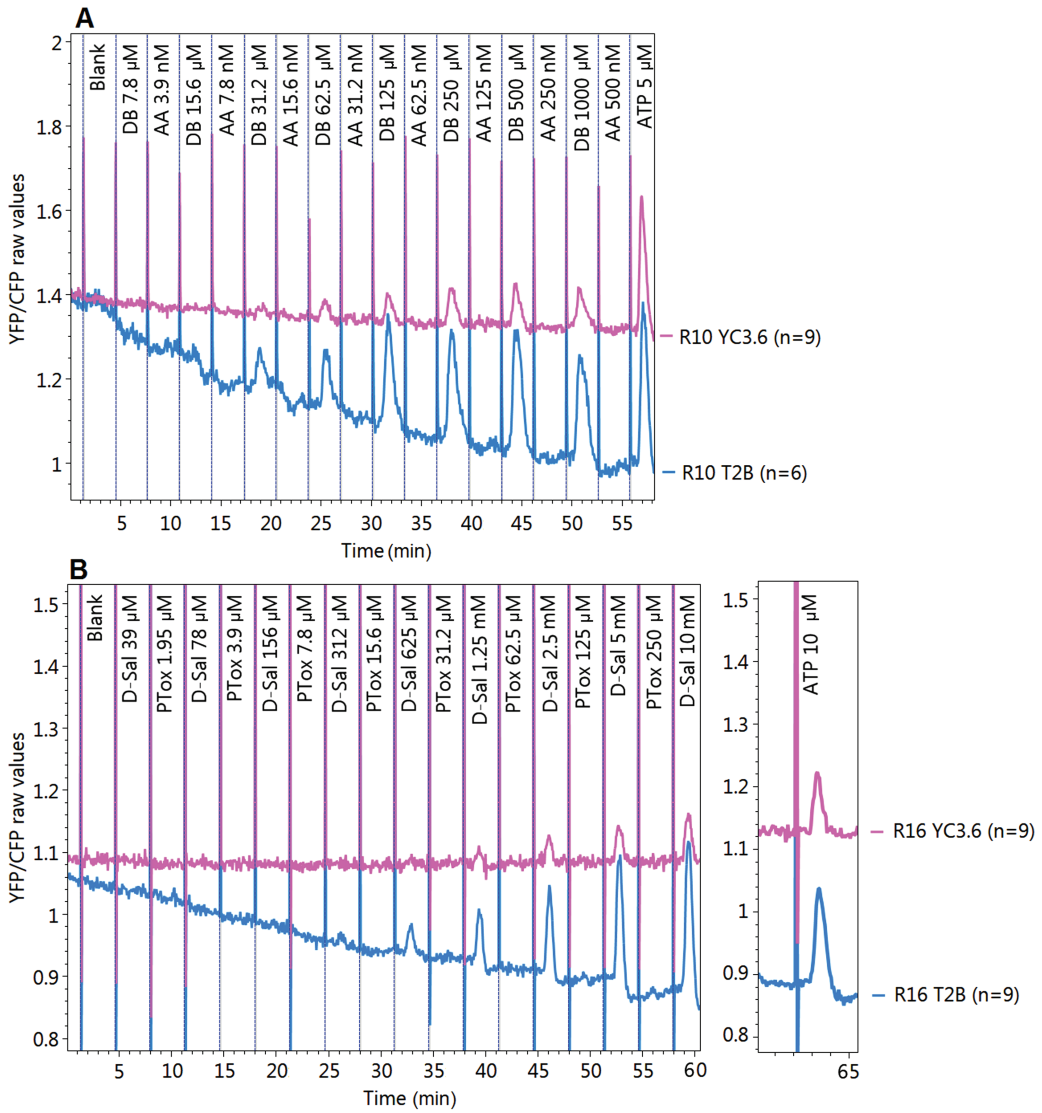

Figure 3. Averaged raw traces YFP FRET/CFP from (**A**) TAS2R10 and denatonium benzoate (DB) and (**B**) TAS2R16 and D-salicin. Traces are shown for both Twitch2B (T2B) and YC3.6 sensor combination. Agonist injections were alternated every 3 min and agonist exposure was approximately 30 s. The lines represent averages of 6–9 replicated spots as indicated in the legends of the charts. AA, aristolochic acid, PTox, picrotoxinin, D-Sal, D-salicin, DB, denatonium benzoate.

Discussion

In this study, we have evaluated the effectiveness of different genetically encoded calcium sensors, at a range of concentrations, for their ability to measure the comparatively low responses of bitter receptors. We observed strong response differences (4- to 5-fold) depending on sensor type and found that sensor Twitch2B yielded the strongest and most sensitive responses for 8 of the evaluated bitter receptors. When compared with YC3.6, sensor Nano140 also yielded an improved calcium sensing, but Twitch2B appeared the best choice for bitter taste receptor arrays. In addition, we found a remarkably strong effect of the calcium sensor concentration on the sensitivity of the response. Lowering the gene dose 4-fold to 8 ng/µL resulted in about 2- to 3-fold lower protein concentrations (Roelse et al. 2018), but improved the sensitivity for all sensors 4- to 15-fold. Doses lower than 8 ng/µL sensor DNA in the print mix yielded arrays with poorly detectable baseline fluorescence (data not shown), and therefore, 8 ng/µL sensor DNA was determined as optimal in our setup. The observed gene dose effects are a clear example of calcium buffering in our reverse transfected cell arrays. Endogenous calcium sensors, naturally present in cells, regulate calcium levels or transduce signals in response to changes in calcium concentration (Clapham 2007; Schwaller 2010). These endogenous sensors bind and buffer part of the calcium, which enters the cytosol. The remaining free calcium ions are available to the fluorescent calcium sensor. This calcium sensor also binds and buffers a fraction of the free calcium. This buffering by fluorescent calcium sensors is problematic when the calcium binding or buffering capacity of the sensor is in the same range or exceeding the calcium buffering capacity of the cell itself (McMahon and Jackson 2018). An effective way of reducing the contribution of this buffering effect and thereby measuring true calcium responses is to lower the fluorescent calcium sensor concentration as much as possible (McMahon and Jackson 2018). Unfortunately, fluorescence-based calcium sensors cannot be diluted too much due to fluorescence noise levels and limitations in detector sensitivity. As argued by McMahon and Jackson (2018), this means that for most genetically encoded and synthetic calcium

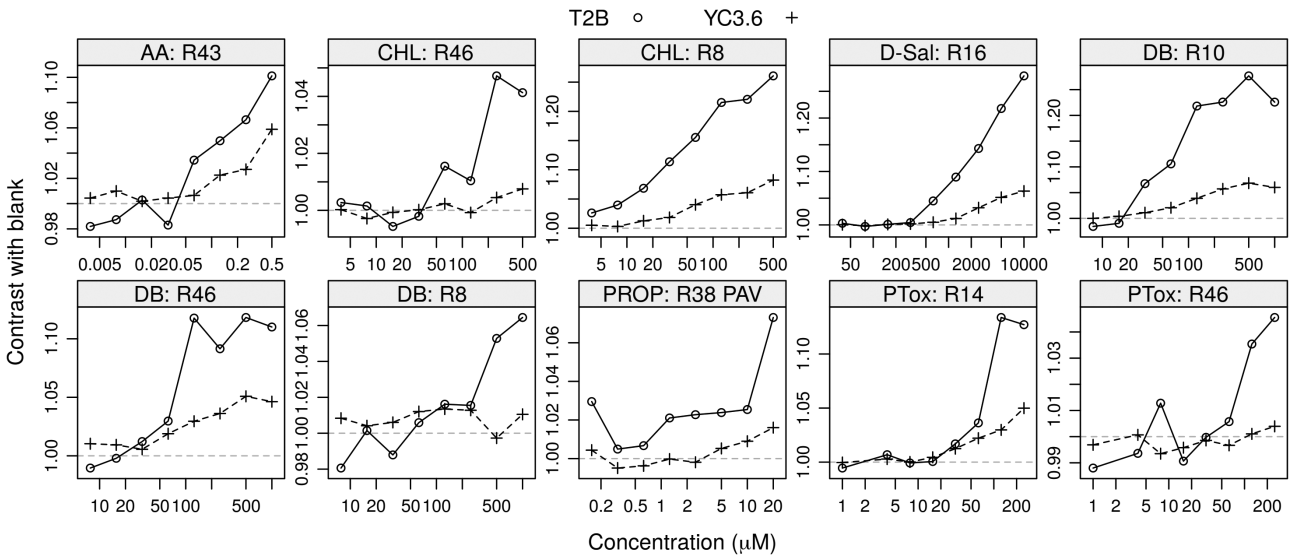

Figure 4. Response curves of Twitch2B (T2B, circles) and YC3.6 (marks) of the responding TAS2R receptor spots from the 3 experiments. The full set of responses is available in Supplementary Figure 3. Response values represent estimates of treatment-versus-control contrasts with respect to the blank injection. AA, aristolochic acid; CHL, chloramphenicol; PTox, picrotoxinin; D-Sal, D-salicin; DB, denatonium benzoate; PROP, 6-*n*-propylthiouracil.

Table 2. Difference in sensitivity for the receptor/agonist combinations with either Twitch2B or YC3.6 sensor transfected at DNA concentration of 8 ng/μL

Receptor	Agonist	Response range[a] of Twitch2B	Response range[a] of YC3.6	Fold increase in sensitivity	Reference EC50 values
TAS2R8	Chloramphenicol	3.9–125 μM	31.2–500 μM	8	n.d.
	Denatonium benzoate	250–1000 μM	—		n.d.
TAS2R10	Denatonium benzoate	15.6–125 μM	125–500 μM	8	59 μM ± 30 (Born et al. 2013)
TAS2R14	Picrotoxinin	31.2–250 μM	62.5–250 μM	2	18 μM (Behrens et al. 2004)
TAS2R16	D-salicin	0.312–10 mM	1.25–10 mM	4	1.2 mM (Greene et al. 2011); 1.1 mM ± 0.3 (Bufe et al. 2002)
TAS2R38 PAV	PROP (6-*n*-propylthiouracil)	10–20 μM	—		2.1 μM (Meyerhof et al. 2011)
TAS2R43	Aristolochic acid	62.5–500 nM	250–500 nM	4	81 nM ± 0.0008 (Kuhn et al. 2004)
TAS2R46	Picrotoxinin	62.5–250 μM	—		70 μM ± 5.2 (Brockhoff et al. 2007)
	Chloramphenicol	125–500 μM	—		n.d.
	Denatonium benzoate	62.5–125 μM	250–500 μM	4	240 μM ± 192 (Brockhoff et al. 2007)

n.d., EC50 not determined, but activation published in Meyerhof et al. (2010).
[a]Concentration range in which an increasing response trend is observed.

fluorophores, the observed calcium dynamics are quenched even under our more optimal low probe conditions. A future solution would be to switch to bioluminescence-based detection platforms for the measurement of cell calcium ion levels (Yang et al. 2016). Photodetectors are generally regarded as 10–1000 times more sensitive than fluorescence detectors (Kim 2016), allowing a further reduction in the amount of sensor needed for calcium detection and minimizing the calcium buffering.

Using optimal sensor concentrations, the 2 sensor types, Twitch2B and YC3.6, were compared on sensitivity performance for a range of bitter taste receptors. The sensitivity was benchmarked against the EC50 values obtained from the literature studies employing calcium dyes, for each receptor–agonist pair. Except for the combinations TAS2R14/TAS2R46 with picrotoxinin and TAS2R38PAV with PROP, the published EC50 values are comparable to the response range obtained with receptor-Twitch2B combinations. The TAS2R46 response range to denatonium benzoate was lower than published. Deviations from the published values may relate to SNP variant differences (Supplementary Table 1) or to differences in the quality of the ligand stock solutions. Also, the sensitivity of our specific imaging setup (filter, lens, and camera) may play a role in missing very small effects. We rule out that it relates to lack of sensitivity of the Twitch2B probe because we show it is capable of following the modulation (lowering) of the resting concentration of cytosolic calcium (Figure 4).

The observed effects of the sensor type for sensors with similar dissociation constants can be explained by differences in the cooperative binding of calcium. Sensors with a Hill coefficient > 1 have smaller ratio changes at calcium levels below their K_d because of the sigmoidal shape of the calcium binding curve. We have confirmed this by comparing the calcium affinity curves of Twitch2B and YC3.6. The R_{min} of Twitch2B was found to be well below the resting calcium level of the HEK293 cells, whereas the YC3.6 sensor did not show a clear decrease in R_{min} after chelating all calcium ions. With a sensitivity range that includes the resting values, the Twitch2B sensor is sensitive to minor changes in calcium. This makes it well suited for

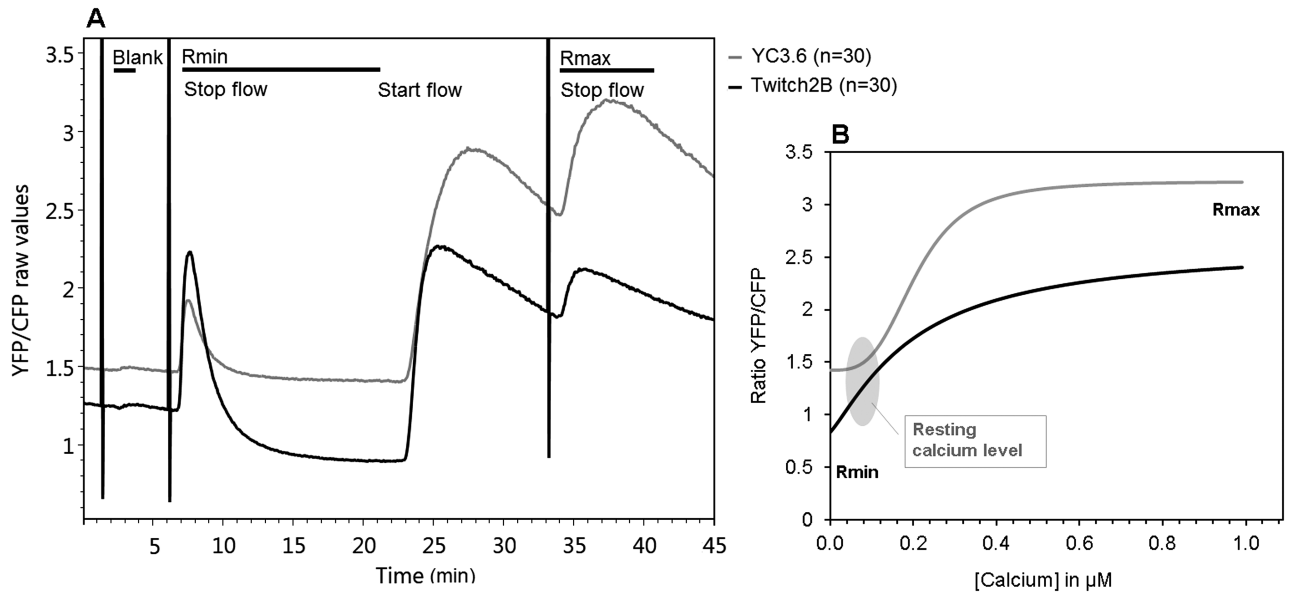

Figure 5. (**A**) Raw traces YFP FRET/CFP from spots expressing either Twitch2B or YC3.6. The flow was set at 200 µL/min C1 buffer. After a blank injection, the R_{min} buffer (C1 buffer without $CaCl_2$ but supplemented with 3 mM EGTA and 5 µM ionomycin) was injected. The flow was stopped at full R_{min} exposure and incubated for 15 min. Next, the flow was started again replacing the R_{min} buffer with the C1 buffer. Approximately 10 min later the R_{max} buffer (C1 buffer with 5 mM $CaCl_2$ and 5 µM Ionomycin) was injected and the flow was stopped at full R_{max} exposure. (**B**) Calculated theoretical calcium binding curves for YC3.6 and Twitch2B based on R_{min} and R_{max} measurements, the known dissociation constants for calcium and the Hill equation (see Materials and methods section).

relatively weak responses to receptor agonists or inverse agonists as in case of bitter receptors. Furthermore, it has a more linear ratio increase so that it is less biased for a certain concentration range.

Twitch2B may be less suitable for detecting calcium dynamics above 300 nM (as observed for some hormone receptors or ion channels) because, in that range, the sensor will become saturated (Figure 5; Thestrup et al. 2014). YC3.6 may not be a good alternative for such receptors either, but other probes might be considered with a K_d in the range of >400 nM (Lindenburg and Merkx 2014; Ma et al. 2017; Ni et al. 2018). Twitch2B may also be less suitable for application in ion-channel arrays because "leaky" calcium ion channels can increase the resting levels of calcium within the cells (Nishihara et al. 2011). Consequently, depending on the expected calcium signaling range, a well-considered choice of calcium sensor type has the potential to improve the sensitivity of the measurements although the linearity of the response from the resting level up (or down) is always an issue that should be taken into account.

Conclusion

Overall, we conclude that by choosing sensor Twitch2B in a bitter receptor array, we could enhance the sensitivity of bitter taste receptor arrays up to 60-fold compared with the more standard YC3.6. The response height increased 5- to 10-fold when the sensor concentration was also optimized. The receptor cell array contained 300 spots and could be exposed to a series of 18 injections within 1 h. A triplicate experiment lasting 3 h represents a high-throughput analysis comprising 16 200 measurements and thus makes receptomics using flow cells a viable alternative to microtiter plate platforms. These optimized sensor conditions, together with a flow-through microfluidic format, will benefit future receptomics experiments involving receptor cell arrays.

Supplementary material

Supplementary data are available at *Chemical Senses* online.

Supplementary Figure 1. Response values of TAS2R8 and TAS2R14 for stimulation with agonist mixture (chloramphenicol and picrotoxinin) for both arrays at sensor gene dose of 8, 16 and 25 ng/µL. Error bars present the 95% confidence interval of the response value. Response values represent estimates of treatment-versus-control contrasts with respect to the 1 µM injection. Abbreviations: T2B = Twitch2B

Supplementary Figure 2. Relationship between total DNA and receptor (TAS2R14) coding DNA in the print mix. The calcium sensor Twitch2B was added to the mix at 8 ng/µL. Abbreviations: PTox = picrotoxinin.

Supplementary Figure 3. Response values of TAS2R and mock spots stimulated with alternating injected samples. Each series is measured on a separate array. Error bars present the 95% confidence interval of the response value. Response values represent estimates of treatment-versus-control contrasts with respect to the blank injection. Sets with less than 5 spots were excluded. YC- control for optical changes (air bubbles, autofluorescence etc.) is a deletion mutant of YC3.6 (Δ A332-S392) with fixed FRET between CFP and YFP. Abbreviations: T2B = Twitch2B, AA = aristolochic acid, CHL = chloramphenicol, PTox = picrotoxinin, D-Sal = D-salicin, DB = denatonium benzoate and PROP = 6-n-propylthiouracil.

Supplementary Figure 4. Metabolic exhaustion measurement by ATP exposure at the end of each injection series. ATP responses were compared with the blank for all bitter receptor spot types combined with either Twitch2B (**A**) or YC3.6 (**B**) for the 3 arrays. Array 1 was exposed to 10 µM ATP for and arrays 2 and 3 to 5 µM ATP. Array 1 featured alternating injections of D-salicin and picrotoxinin which activated TAS2R16 and TAS2R14/TAS2R46. Array 2 featured alternating injections of chloramphenicol and PROP which activated TAS2R8/TAS2R46 and TAS2R38PAV. Array 3 featured alternating injections of aristolochic acid and denatonium benzoate which activated TAS2R43 and TAS2R8/TAS2R10/TAS2R46. Error bars show a 95% confidence interval for the response estimates.

Supplementary Table 1. Bitter taste receptor genes.

Funding

This work was supported by the Dutch Topsector Horticulture and Propagation Materials, project "HTP phenotyping tomato flavour" KV 1409-025.

Acknowledgments

Imaging facilities were offered by the Cell Biology and Immunology Group of Animal Sciences at WUR. Data analysis and visualization software was written by Marco van Lenthe from BU Biometris, Wageningen University and Research.

Author contributions

Conceptualization: M.R. and M.A.J. Data curation: M.R. Data analysis: M.R. and R.W. Funding acquisition: M.A.J. Gene cloning: M.G.L.H. and M.R. Writing (original draft preparation): M.R., R.W., and M.A.J. Writing (review and editing): M.R., M.A.J., R.W., M.G.L.H., R.DH., and R.F.W.

Conflict of interest

All authors declare no conflicts of interest. The founding sponsors had no role in the design of the study; in the collection, analyses, or interpretation of data; in the writing of the manuscript, and in the decision to publish the results.

References

Behrens M, Bartelt J, Reichling C, Winnig M, Kuhn C, Meyerhof W. 2006. Members of RTP and REEP gene families influence functional bitter taste receptor expression. *J Biol Chem*. 281:20650–20659.

Behrens M, Brockhoff A, Kuhn C, Bufe B, Winnig M, Meyerhof W. 2004. The human taste receptor hTAS2R14 responds to a variety of different bitter compounds. *Biochem Biophys Res Commun*. 319:479–485.

Behrens M, Meyerhof W. 2013. Bitter taste receptor research comes of age: from characterization to modulation of TAS2Rs. *Semin Cell Dev Biol*. 24:215–221.

Born S, Levit A, Niv MY, Meyerhof W, Behrens M. 2013. The human bitter taste receptor TAS2R10 is tailored to accommodate numerous diverse ligands. *J Neurosci*. 33:201–213.

Brockhoff A, Behrens M, Massarotti A, Appendino G, Meyerhof W. 2007. Broad tuning of the human bitter taste receptor hTAS2R46 to various sesquiterpene lactones, clerodane and labdane diterpenoids, strychnine, and denatonium. *J Agric Food Chem*. 55:6236–6243.

Bufe B, Hofmann T, Krautwurst D, Raguse JD, Meyerhof W. 2002. The human TAS2R16 receptor mediates bitter taste in response to beta-glucopyranosides. *Nat Genet*. 32:397–401.

Bufe B, Scholey-Pohl E, Krautwurst D, Hofmann T, Meyerhof W. 2004. Identification of human bitter taste receptors. *ACS Sym Ser*. 867:45–59.

Chandrashekar J, Mueller KL, Hoon MA, Adler E, Feng L, Guo W, Zuker CS, Ryba NJ. 2000. T2Rs function as bitter taste receptors. *Cell*. 100:703–711.

Clapham DE. 2007. Calcium signaling. *Cell*. 131:1047–1058.

Devillier P, Naline E, Grassin-Delyle S. 2015. The pharmacology of bitter taste receptors and their role in human airways. *Pharmacol Ther*. 155:11–21.

Gadagkar SR, Call GB. 2015. Computational tools for fitting the Hill equation to dose–response curves. *J Pharmacol Toxicol Methods*. 71:68–76.

Goedhart J, von Stetten D, Noirclerc-Savoye M, Lelimousin M, Joosen L, Hink MA, van Weeren L, Gadella TW Jr, Royant A. 2012. Structure-guided evolution of cyan fluorescent proteins towards a quantum yield of 93%. *Nat Commun*. 3:751.

Greene TA, Alarcon S, Thomas A, Berdougo E, Doranz BJ, Breslin PA, Rucker JB. 2011. Probenecid inhibits the human bitter taste receptor TAS2R16 and suppresses bitter perception of salicin. *PLoS One*. 6:e20123.

Horikawa K, Yamada Y, Matsuda T, Kobayashi K, Hashimoto M, Matsuura T, Miyawaki A, Michikawa T, Mikoshiba K, Nagai T. 2010. Spontaneous network activity visualized by ultrasensitive Ca^{2+} indicators, yellow Cameleon-Nano. *Nat Methods*. 7:729–732.

Kamentsky L, Jones TR, Fraser A, Bray MA, Logan DJ, Madden KL, Ljosa V, Rueden C, Eliceiri KW, Carpenter AE. 2011. Improved structure, function and compatibility for CellProfiler: modular high-throughput image analysis software. *Bioinformatics*. 27:1179–1180.

Kim SB. 2016. *Bioluminescence: methods and protocols*. New York: Springer Science+Business Media New York.

Kuhn C, Bufe B, Batram C, Meyerhof W. 2010. Oligomerization of TAS2R bitter taste receptors. *Chem Senses*. 35:395–406.

Kuhn C, Bufe B, Winnig M, Hofmann T, Frank O, Behrens M, Lewtschenko T, Slack JP, Ward CD, Meyerhof W. 2004. Bitter taste receptors for saccharin and acesulfame K. *J Neurosci*. 24:10260–10265.

Lindenburg L, Merkx M. 2014. Engineering genetically encoded FRET sensors. *Sensors (Basel)*. 14:11691–11713.

Lossow K, Hübner S, Roudnitzky N, Slack JP, Pollastro F, Behrens M, Meyerhof W. 2016. Comprehensive analysis of mouse bitter taste receptors reveals different molecular receptive ranges for orthologous receptors in mice and humans. *J Biol Chem*. 291:15358–15377.

Lu P, Zhang CH, Lifshitz LM, ZhuGe R. 2017. Extraoral bitter taste receptors in health and disease. *J Gen Physiol*. 149:181–197.

Ma Q, Ye L, Liu H, Shi Y, Zhou N. 2017. An overview of Ca^{2+} mobilization assays in GPCR drug discovery. *Expert Opin Drug Discov*. 12:511–523.

Mank M, Griesbeck O. 2008. Genetically encoded calcium indicators. *Chem Rev*. 108:1550–1564.

McCombs JE, Palmer AE. 2008. Measuring calcium dynamics in living cells with genetically encodable calcium indicators. *Methods*. 46:152–159.

McMahon SM, Jackson MB. 2018. An inconvenient truth: calcium sensors are calcium buffers. *Trends Neurosci*. 41:880–884.

Meyerhof W, Batram C, Kuhn C, Brockhoff A, Chudoba E, Bufe B, Appendino G, Behrens M. 2010. The molecular receptive ranges of human TAS2R bitter taste receptors.: *Chem Senses*. 35157–170.

Meyerhof W, Born S, Brockhoff A, Behrens M. 2011. Molecular biology of mammalian bitter taste receptors. A review. *Flavour Frag J*. 26:260–268.

Miyawaki A, Llopis J, Heim R, McCaffery JM, Adams JA, Ikura M, Tsien RY. 1997. Fluorescent indicators for Ca^{2+} based on green fluorescent proteins and calmodulin. *Nature*. 388:882–887.

Miyawaki A, Nagai T, Mizuno H. 2013. Imaging intracellular free Ca^{2+} concentration using yellow cameleons. *Cold Spring Harbor Protocols*. 2013:882–887.

Nagai T, Yamada S, Tominaga T, Ichikawa M, Miyawaki A. 2004. Expanded dynamic range of fluorescent indicators for Ca^{2+} by circularly permuted yellow fluorescent proteins. *Proc Natl Acad Sci USA*. 101:10554–10559.

Narukawa M, Noga C, Ueno Y, Sato T, Misaka T, Watanabe T. 2011. Evaluation of the bitterness of green tea catechins by a cell-based assay with the human bitter taste receptor hTAS2R39. *Biochem Biophys Res Commun*. 405:620–625.

Ni Q, Mehta S, Zhang J. 2018. Live-cell imaging of cell signaling using genetically encoded fluorescent reporters. *FEBS J*. 285:203–219.

Nishihara E, Hiyama TY, Noda M. 2011. Osmosensitivity of transient receptor potential vanilloid 1 is synergistically enhanced by distinct activating stimuli such as temperature and protons. *PLoS One*. 6:e22246.

Ozeck M, Brust P, Xu H, Servant G. 2004. Receptors for bitter, sweet and umami taste couple to inhibitory G protein signaling pathways. *Eur J Pharmacol*. 489:139–149.

Reichling C, Meyerhof W, Behrens M. 2008. Functions of human bitter taste receptors depend on N-glycosylation. *J Neurochem*. 106:1138–1148.

Roelse M, Henquet MGL, Verhoeven HA, de Ruijter NCA, Wehrens R, van Lenthe MS, Witkamp RF, Hall RD, Jongsma MA. 2018. Calcium imaging of GPCR activation using arrays of reverse transfected HEK293 cells in a microfluidic system. *Sensors*. 18.

Rose T, Goltstein PM, Portugues R, Griesbeck O. 2014. Putting a finishing touch on GECIs. *Front Mol Neurosci*. 7:88.

Schwaller B. 2010. Cytosolic Ca^{2+} buffers. *Cold Spring Harb Perspect Biol*. 2:a004051.

Thestrup T, Litzlbauer J, Bartholomäus I, Mues M, Russo L, Dana H, Kovalchuk Y, Liang Y, Kalamakis G, Laukat Y, et al. 2014. Optimized ratiometric calcium sensors for functional in vivo imaging of neurons and T lymphocytes. *Nat Methods*. 11:175–182.

Tong J, McCarthy TV, MacLennan DH. 1999. Measurement of resting cytosolic Ca^{2+} concentrations and Ca^{2+} store size in HEK-293 cells transfected with malignant hyperthermia or central core disease mutant Ca^{2+} release channels. *J Biol Chem*. 274:693–702.

Wehrens R, Roelse M, Henquet M, van Lenthe M, Goedhart PW, Jongsma MA. 2019. Statistical models discriminating between complex samples measured with microfluidic receptor-cell arrays. *PLoS One*. 14:e0214878.

Wettschureck N, Offermanns S. 2005. Mammalian G proteins and their cell type specific functions. *Physiol Rev*. 85:1159–1204.

Yang J, Cumberbatch D, Centanni S, Shi SQ, Winder D, Webb D, Johnson CH. 2016. Coupling optogenetic stimulation with NanoLuc-based luminescence (BRET) Ca++ sensing. *Nat Commun*. 7:13268.

Zhao Y, Araki S, Wu J, Teramoto T, Chang YF, Nakano M, Abdelfattah AS, Fujiwara M, Ishihara T, Nagai T, et al. 2011. An expanded palette of genetically encoded Ca^{2+} indicators. *Science*. 333:1888–1891.